



UNIVERSITY OF CALIFORNIA  
SANTA BARBARA

**Controlling Canards Using Ideas From The Theory of Mixed-Mode  
Oscillations**

by

Joseph William Durham

A thesis submitted in partial satisfaction of the  
requirements for the degree of  
Master of Science

in

Mechanical Engineering

Committee in charge:  
Professor Jeffrey Moehlis, Chair  
Professor Francesco Bullo  
Professor Mustafa Khammash

June 2007

The Thesis of Joseph William Durham is approved:

---

Professor Francesco Bullo

---

Professor Mustafa Khammash

---

Professor Jeffrey Moehlis, Chair

June 2007

**Controlling Canards Using Ideas From The Theory of Mixed-Mode  
Oscillations**

Copyright 2007

by

Joseph William Durham

## **Abstract**

Controlling Canards Using Ideas From The Theory of Mixed-Mode Oscillations

by

Joseph William Durham

Canards are special types of periodic orbits that are associated with a dramatic change in amplitude and period due to a very small change in a parameter. Since canards typically exist only for very small regions of parameter space, they are extremely difficult to observe experimentally. In this thesis we present a continuous feedback control mechanism which uses only the instantaneous position of the system in phase space to tune a system parameter to a value for which a canard exists. This involves controlling a slow variable to drift toward the canard parameter region, much as is the case for mixed-mode oscillations. We apply this to tune the FitzHugh-Nagumo model to produce maximal canard orbits. A system tuned to be at a parameter value where a canard exists could serve as a sensor which could detect extremely small parameter changes. When the controller is improperly configured, periodic or chaotic mixed-mode oscillations are found. We also investigate the effects of noise on this control mechanism.

To Drew

# Contents

<b>List of Figures</b>	<b>vii</b>
<b>1 Introduction</b>	<b>1</b>
1.1 Canards . . . . .	5
1.2 Predicting parameter values at which Hopf bifurcation occurs . .	10
1.3 Predicting parameter values at which canards occur . . . . .	11
<b>2 Control Method</b>	<b>16</b>
2.1 Comparing the Effectiveness of Strategies . . . . .	18
<b>3 Results</b>	<b>21</b>
3.0.1 Mixed-Mode Oscillations and Chaos . . . . .	23
3.1 Robustness . . . . .	30
3.2 Simulations With Noise . . . . .	33
3.2.1 Stochastic Integration method . . . . .	33
3.2.2 Results With Noise . . . . .	35
<b>4 Conclusion</b>	<b>37</b>
<b>Bibliography</b>	<b>39</b>
<b>A Appendix</b>	<b>46</b>

# List of Figures

1.1	Bifurcation diagrams showing fixed point (f.p.) and periodic orbit (p.o.) branches for (a) supercritical Hopf bifurcation, (b) subcritical Hopf bifurcation, (c) canard transition. Solid (resp., dashed) lines indicate stable (resp., unstable) solutions. The parameter changes along the horizontal axis, and the vertical axis is a measure of the size of the periodic orbit. . . . .	4
1.2	Bifurcation diagram from simulations of the FHN model, showing a stable fixed point (f.p.) spawning a stable periodic orbit (p.o.) through a supercritical Hopf bifurcation at $I = 0.0553$ . The size of the periodic orbit is displayed using the maximum value of $v$ along the orbit. A canard transition occurs around $I = 0.0568$ , where the size of the orbit increases sharply over a very narrow range of $I$ . Solid (respectively, dashed) lines represent stable (respectively, unstable) solutions. . . . .	6
1.3	Stable periodic orbit evolution over a small range of parameter $I$ in the FHN model: (a) $I = 0.056838$ , (b) $I = 0.05683845$ , (c) $I = 0.05683848$ , (d) $I = 0.05683858$ , (e) $I = 0.05684$ . Here, and in later phase plane figures, the dashed line is the $v$ -nullcline where $f(v, w) = 0$ . . . . .	7
1.4	Two different values of $I$ producing different dynamics for the system. In (a), a lower value of $I$ produces a single stable fixed point. In (b), a higher value of $I$ produces a large stable periodic orbit. The intersection of the $v$ and $w$ -nullclines has shifted from the left side of the local minimum of the $v$ -nullcline to the right side. . . . .	8
1.5	The two generic situations for the relative positions of the slow manifolds $M_S$ and $M_U$ near the local minimum of the $v$ -nullcline. A trajectory follows $M_S$ , and after passing near the local minimum of the $v$ -nullcline either (a) returns quickly to a neighborhood of $M_S$ , or (b) undergoes a large excursion before returning to a neighborhood of $M_S$ . . . . .	10

2.1	Demonstration of how our distance measure classifies several trajectories. The dashed line is the $v$ -nullcline, within $O(\epsilon)$ of $M_U$ . The thicker part of the trajectories count towards the distance following $M_U$ , the thinner pieces do not. Here, the longest distance is approximately 0.6, the shortest 0.15. . . . .	19
3.1	Contour plot of the average distance the trajectories remain in the neighborhood of $M_U$ after transients have died out. Average is taken over at least 40 successive visits near $M_U$ . . . . .	22
3.2	This canard trajectory, produced using control with $c = 1 \times 10^{-8}$ and $r_0 = 0.234$ , has the longest distance measure along $M_U$ . The axes are not square, so the dot-dashed control circle appears elliptical. . . . .	24
3.3	Evolution of $I$ for the trajectory in Fig. 3.2. . . . .	24
3.4	Bifurcation diagram for $c = 1 \times 10^{-8}$ showing peak values of $v$ , generated by adiabatically increasing the value of $r_0$ , omitting transients. There is a period two bubble corresponding to a MMO with one small and one large orbit as $r$ is swept from 0.18 to 0.25. The maximal canard has $v_{peak} \approx 0.65$ . . . . .	25
3.5	Bifurcation diagram, as in Fig. 3.4, for (a) $c = 2 \times 10^{-8}$ , (b) $c = 5 \times 10^{-8}$ , (c) $c = 1 \times 10^{-7}$ , all showing period doubling cascades to chaos and various periodic windows corresponding to periodic MMO. The maximal canard has $v_{peak} \approx 0.65$ . . . . .	27
3.6	Control with $c = 1 \times 10^{-7}$ and $r_0 = 0.17$ produces a chaotic MMO. . . . .	28
3.7	Three dimensional representation of the chaotic trajectory from Fig. 3.6, with the $(v, w)$ -phase plane augmented with a dimension for $I$ . The cubic $v$ -nullcline is now the two dimensional surface $S$ with fold-line $F$ . . . . .	29
3.8	Map of peak value of $v$ in Fig. 3.6 versus the previous peak. This one dimensional map shows that the spread of orbits in Fig. 3.6 is due to chaos. . . . .	29
3.9	Contour plot with the same setup as Fig. 3.1 except that the center of the control circle has been displaced to $(0.12, 0.08)$ . The two contours are nearly identical despite the translated control circle. . . . .	31
3.10	(a) Control variable $I$ first locates initial canard window for $\gamma = 1.0$ . After it achieves a lock, $\gamma$ is reduced to 0.985 and $I$ then tunes to the new canard window at $I = 0.05764$ , as confirmed by simulations. (b) The control strength $c$ is varied based on recent history of $I$ . . . . .	32

3.11 Noisy MMO produced using  $c = 1 \times 10^{-8}$ ,  $r_0 = 0.234$  and noise strength  $D = 1 \times 10^{-11}$ . This is the same controller that produced the best canard in Fig. 3.2. With noise, the controller can only find the general location of the canard window; the continuous noise precludes actual canard trajectories. . . . . 36

## Acknowledgments

I wish to acknowledge and thank my advisor, Dr. Jeff Moehlis, for his encouragement and advice over the last year. This thesis was inspired by the material and final project from one of his classes, but it is his guidance beyond the technical material that will serve me best in my future work.

I would also like to thank my parents. They have never pushed me in a particular direction, but instead provided a great foundation and support for whatever path I chose.

Finally, I would like to thank my wife for her love and understanding that have made the last two years truly wonderful.

# Chapter 1

## Introduction

Canards are periodic orbits for which the trajectory follows both attracting and repelling slow manifolds. They are associated with a dramatic change in amplitude and period over a very narrow interval of a parameter. Canards may be present in singularly perturbed systems of ordinary differential equations: a common scenario in which they arise is that a “small” stable periodic orbit is born in a supercritical Hopf bifurcation and rapidly changes to a “large” relaxation oscillation periodic orbit as a parameter is varied. Canards are the intermediate periodic orbits between the small and large orbits. The shape of these periodic orbits in phase space can resemble a duck, hence the name “canard,” the French word for duck. Canards were first found in studies of the van der Pol system [3, 10, 15], and have since been found and analyzed to varying degrees for a variety of chemical, biological, and other systems [1, 2, 4, 8, 6, 7, 14, 24, 33, 34, 37, 38, 41, 42, 48, 45, 50, 52]. Because canards typically only exist for

very small regions of parameter space, they are extremely difficult to observe experimentally.

We present a control mechanism which tunes a system to be at a parameter value for which a canard exists. This is a continuous feedback control law which uses only the instantaneous position of the system in phase space, and is conceptually similar to one approach used for tuning a system to be at a Hopf bifurcation [43]. Our control mechanism exploits the relationship of canards to mixed-mode oscillations (MMO), which are solutions consisting of sequences of “small” and “large” orbits in phase space, as determined by whether the traced orbits are “smaller” or “larger” than the corresponding canard solutions. MMO have been found and analyzed for various systems; see [13, 18, 32, 39, 40, 46]. MMO occur, for example, for fast-slow dynamical systems when a variable on average slowly drifts toward a transition from its present state (tracing a large or small orbit) to a different state (tracing a small or large orbit). Most commonly, such transitions occur periodically, giving MMO which can be characterized by the repeating sequence in which the small and large orbits occur, although chaotic MMO can also occur. Our control mechanism involves a slow variable which similarly drifts toward the canard transition.

A system tuned to be at or near a parameter value for which a transition occurs, such as a bifurcation or canard transition, can be used to sense parameter changes: one type of behavior indicates the parameter changed in one direction,

while another type of behavior indicates the parameter changed in the other direction. For example, suppose a system is tuned to be at a parameter value at which a supercritical Hopf bifurcation occurs, as in Fig. 1.1(a). (For methods for tuning to a Hopf bifurcation, see [43, 35]; for applications to non-linear amplification in hearing and hair cells in the cochlea, see [11, 16, 17, 36].) If the parameter decreases a stable fixed point will be reached, while if the parameter increases a stable periodic orbit will be reached. However, for Hopf bifurcations the size of the periodic orbit shrinks to zero as bifurcation is approached; if it is difficult to distinguish a fixed point from a small periodic orbit, such a system would have trouble detecting small parameter changes.

On the other hand, suppose that a system is tuned to be at a parameter value at which a subcritical Hopf bifurcation occurs, with the periodic orbit gaining stability in a saddlenode bifurcation, as in Fig. 1.1(b). If the parameter increases even a small amount, a large periodic orbit will be reached, which might be easily distinguished from a stable fixed point. However, such a system would not easily detect a subsequent small decrease in the parameter: hysteresis makes the system stay on the stable periodic orbit branch. In order to “reset” such a sensor, it would be necessary to decrease the parameter by a substantial amount (past the saddlenode bifurcation), then re-tune the system to be at the subcritical Hopf bifurcation.

In contrast, consider a system which is tuned to be at a parameter value for

which a canard exists, as in Fig. 1.1(c). The presence of a “large” periodic orbit indicates a positive change in the parameter, while the presence of a “small” periodic orbit indicates a negative change in the parameter. Note that, because of the nature of the canard transition, this will be true even for very small changes in the parameters. If it is relatively easy to distinguish a large from a small periodic orbit, such a sensor could detect extremely small parameter changes while avoiding issues with hysteresis.

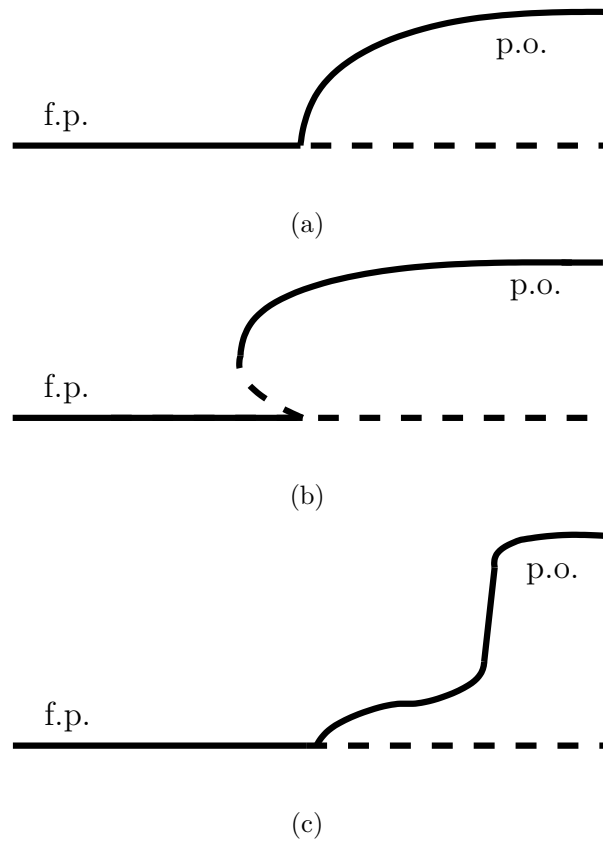


Figure 1.1: Bifurcation diagrams showing fixed point (f.p.) and periodic orbit (p.o.) branches for (a) supercritical Hopf bifurcation, (b) subcritical Hopf bifurcation, (c) canard transition. Solid (resp., dashed) lines indicate stable (resp., unstable) solutions. The parameter changes along the horizontal axis, and the vertical axis is a measure of the size of the periodic orbit.

In the development of our control method, we begin in Section 1.1 by dis-

cussing the presence of canards in the FitzHugh-Nagumo model, a prototypical model for neural dynamics which will serve as the example throughout this thesis. We derive an approximation for the location of canards in the FitzHugh-Nagumo model using singular perturbation theory in Section 1.3. In Chapter 2, we describe the control mechanism which tunes our system to be at a parameter value for which canards exist. Next, in Chapter 3, we determine how well the control works for different parameters in the control law. This includes the result that for certain parameters, the control law leads to MMO. We also consider this control mechanism for this system subjected to white noise in Section 3.2. While we focus on the FitzHugh-Nagumo equations, we expect that the mechanism which we describe will work for other systems, provided appropriate tuning of the parameters in the control law is done.

## 1.1 Canard Basics

The system we consider is the FitzHugh-Nagumo (FHN) model of neuron spiking behavior [22, 44, 31]. The dynamics are described by the differential equations

$$\dot{v} = -w - v(v - 1)(v - a) + I \equiv f(v, w; I), \quad (1.1)$$

$$\dot{w} = \epsilon(v - \gamma w) \equiv \epsilon g(v, w). \quad (1.2)$$

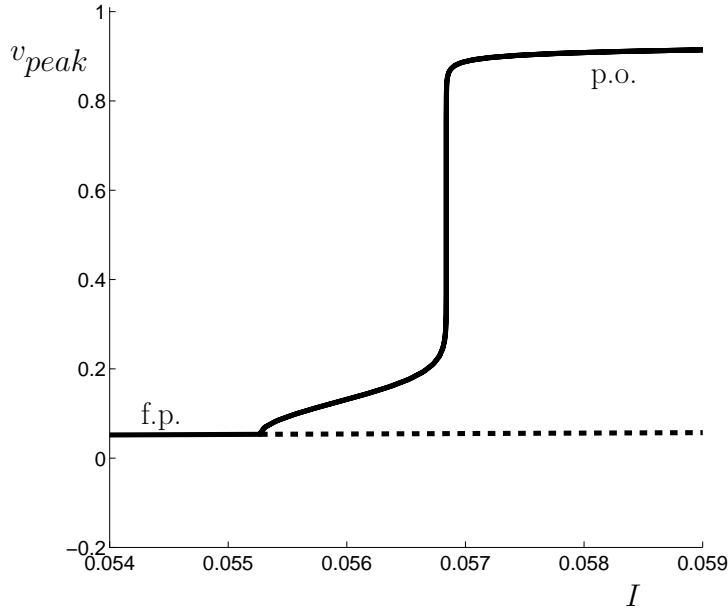


Figure 1.2: Bifurcation diagram from simulations of the FHN model, showing a stable fixed point (f.p.) spawning a stable periodic orbit (p.o.) through a supercritical Hopf bifurcation at  $I = 0.0553$ . The size of the periodic orbit is displayed using the maximum value of  $v$  along the orbit. A canard transition occurs around  $I = 0.0568$ , where the size of the orbit increases sharply over a very narrow range of  $I$ . Solid (respectively, dashed) lines represent stable (respectively, unstable) solutions.

Here,  $\epsilon \ll 1$  is a time-scale separation parameter, and  $v$  and  $w$  refer to voltage and recovery variables, respectively. Following Brøns [5], we set  $a = 0.1$ ,  $\gamma = 1$ , and  $\epsilon = 0.008$ . The parameter  $I$  represents an external current applied to the model, and in this section we treat it as a bifurcation parameter. As shown in Fig. 1.2, the FHN model with these parameters undergoes a supercritical Hopf bifurcation around  $I = 0.0553$ , and shortly thereafter the amplitude and shape of the stable periodic orbit changes dramatically over a very narrow range of  $I$ . This narrow range of  $I$  is the canard region: a sample of canard periodic orbits is shown in Fig. 1.3.

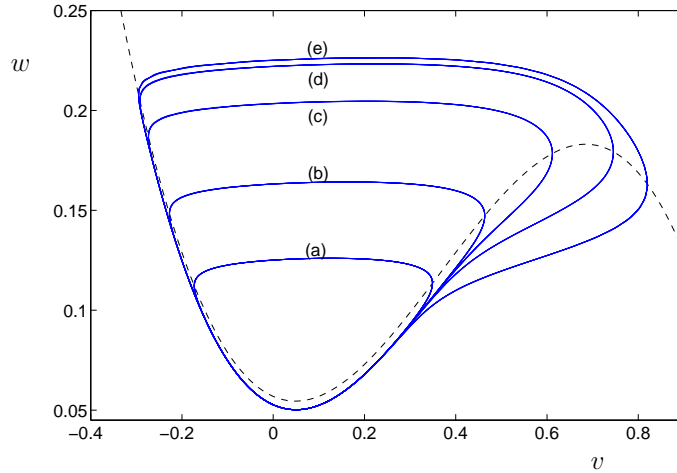


Figure 1.3: Stable periodic orbit evolution over a small range of parameter  $I$  in the FHN model: (a)  $I = 0.056838$ , (b)  $I = 0.05683845$ , (c)  $I = 0.05683848$ , (d)  $I = 0.05683858$ , (e)  $I = 0.05684$ . Here, and in later phase plane figures, the dashed line is the  $v$ -nullcline where  $f(v, w) = 0$ .

The canard phenomenon can be understood as follows. The system has two nullclines, a cubic  $v$ -nullcline where  $\dot{v} = f(v, w) = 0$  and a linear  $w$ -nullcline where  $\dot{w} = g(v, w) = 0$ . As the parameter  $I$  increases, the cubic  $v$ -nullcline translates upwards in  $w$ , causing the intersection of the two nullclines to translate along the  $v$ -nullcline towards higher values of  $v$ . The Hopf bifurcation shown in Fig. 1.2 occurs shortly after the  $w$ -nullcline passes through the local minimum of the  $v$ -nullcline, as demonstrated in Fig. 1.4. The canard region exists in between the Hopf bifurcation and the large stable periodic orbit in Fig. 1.4(b).

Time-scale separation plays a critical role in canard system dynamics. For the FHN model, the tiny parameter  $\epsilon$  causes the  $w$  dynamics to be orders of magnitude slower than the  $v$  dynamics when the system is away from the  $v$ -nullcline. When trajectories approach the  $v$ -nullcline, the  $v$  dynamics shrink

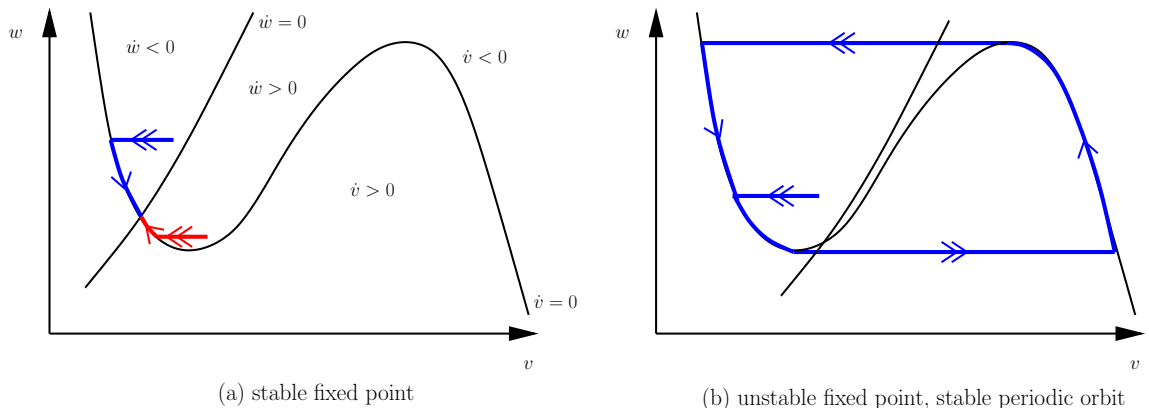


Figure 1.4: Two different values of  $I$  producing different dynamics for the system. In (a), a lower value of  $I$  produces a single stable fixed point. In (b), a higher value of  $I$  produces a large stable periodic orbit. The intersection of the  $v$  and  $w$ -nullclines has shifted from the left side of the local minimum of the  $v$ -nullcline to the right side.

towards 0 and the system operates at the slower time-scale of the  $w$  dynamics.

In Fig. 1.4 double arrows indicate the system is evolving rapidly, while the slower dynamics along the  $v$ -nullcline are represented with a single arrow. For canard trajectories like (c) and (d) in Fig. 1.3, the system spends most of its time near the  $v$ -nullcline, while the traversal across the top happens very quickly.

In order to predict the location for the canard region, we first need to establish the relationship between nullclines and slow manifolds for this system. If  $\epsilon$  is set equal to zero, then  $\dot{w} = 0$ , and the  $v$ -nullcline is a curve of fixed points and is normally hyperbolic on the pieces for which its slope is bounded away from zero, i.e., away from its local minimum and local maximum when plotted in the  $(v, w)$  phase space (see Fig. 1.3). For  $\epsilon = 0$ , the “left” and “right” parts of the  $v$ -nullcline are found to be stable to transverse perturbations, while the “middle” part is found to be unstable to transverse perturbations.

Invariant manifold theorems imply that, for  $\epsilon$  sufficiently small, invariant manifolds persist within  $O(\epsilon)$  of these normally hyperbolic pieces of the  $v$ -nullcline, with the manifolds inheriting their normal stability properties from the stability properties of the pieces of the  $v$ -nullcline [19, 20, 53]. There will thus be a slow manifold  $M_S$ , with stable foliation, within  $O(\epsilon)$  of the “left” part of the  $v$ -nullcline, a different slow manifold, with stable foliation, within  $O(\epsilon)$  of the “right” part of the  $v$ -nullcline, and a slow manifold  $M_U$ , with unstable foliation, within  $O(\epsilon)$  of the “middle” part of the  $v$ -nullcline. The manifolds  $M_S$  and  $M_U$  can be extended beyond the local minimum and local maximum according to the flow, but the extensions may leave an  $O(\epsilon)$  distance of the  $v$ -nullcline, and may also lose their normal stability properties.

Generically, the distance between  $M_S$  and  $M_U$  is nonzero near the local minimum of the  $v$ -nullcline. This distance changes as parameters are varied. For the FHN model, a “small” stable periodic orbit is born in a supercritical Hopf bifurcation, with the manifolds as sketched in Fig. 1.5(a). As  $I$  is increased from the Hopf bifurcation point, the relative position of the manifolds switches to the case sketched in Fig. 1.5(b). For particular parameters the manifolds  $M_S$  and  $M_U$  connect smoothly; for parameters  $O(e^{-K/\epsilon})$  close to this for some  $K > 0$ , the periodic orbit is called a canard, and it follows  $M_U$  for a substantial distance [15, 34]. In the following sections we will first calculate the location of the Hopf bifurcation point, and then, using this connecting manifolds framework,

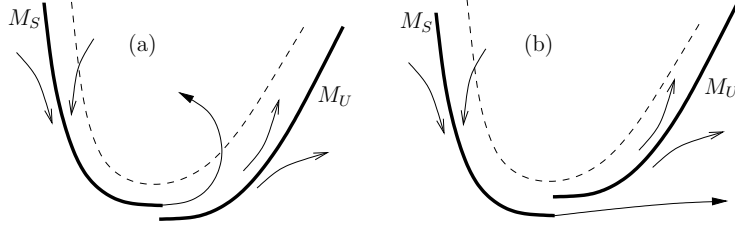


Figure 1.5: The two generic situations for the relative positions of the slow manifolds  $M_S$  and  $M_U$  near the local minimum of the  $v$ -nullcline. A trajectory follows  $M_S$ , and after passing near the local minimum of the  $v$ -nullcline either (a) returns quickly to a neighborhood of  $M_S$ , or (b) undergoes a large excursion before returning to a neighborhood of  $M_S$ .

the canard region.

## 1.2 Predicting parameter values at which Hopf bifurcation occurs

To determine the location of the supercritical Hopf bifurcation for the FHN model, we will first locate the critical point  $(v_{cp}, w_{cp})$  where

$$f(v_{cp}, w_{cp}; I) = g(v_{cp}, w_{cp}) = 0. \quad (1.3)$$

Solving this system yields equations for  $v_{cp}$  and  $w_{cp}$  in terms of  $I$ ,  $\gamma$ , and  $a$ , that we will omit. The Hopf bifurcation occurs when the eigenvalues of the system linearized about this critical point cross the imaginary axis with non-zero speed. Linearizing the FHN model about the critical point yields the following Jacobian matrix:

$$J(I, \epsilon) = \begin{pmatrix} \frac{\partial f}{\partial v} & \frac{\partial f}{\partial w} \\ \epsilon \frac{\partial g}{\partial v} & \epsilon \frac{\partial g}{\partial w} \end{pmatrix} \quad (1.4)$$

where all derivatives are evaluated at  $(v_{cp}, w_{cp})$ . The trace of the Jacobian matrix determines the real part of the eigenvalues of the linearized system. Solving for the value of  $I$  where  $tr(J(I, \epsilon)) = 0$  for our parameters yields the location of the Hopf bifurcation,  $I_H$ :

$$I_H \approx 0.05527. \quad (1.5)$$

This result matches the value found using Eq. 3.10 of Brøns [6]. For this to be a Hopf bifurcation it must also fulfill the following conditions:

$$\det(J(I_H, \epsilon)) > 0, \quad (1.6)$$

$$\frac{\partial \text{tr}(J(I_H, \epsilon))}{\partial I} \neq 0. \quad (1.7)$$

Both of these conditions hold at  $I_H$  for  $\epsilon = 0.008$ .

### 1.3 Predicting parameter values at which canards occur

Singular perturbation theory can be used to predict the parameter values at which manifolds  $M_S$  and  $M_U$  connect to produce a canard trajectory [7, 41, 6]. To locate the canard point  $I_C$ , we expand the parameter  $I$  in powers of  $\epsilon$  about a fixed value  $I_0$  to be defined below:

$$I_C(\epsilon) = I_0 + \epsilon I_1 + h.o.t. \quad (1.8)$$

where *h.o.t.* stand for higher order terms in  $\epsilon$ . We seek an approximation to the connected canard manifold, which defines  $w$  as a function of  $v$  and  $I$ :

$$w(v; I) = w_0(v; I_0) + \epsilon w_1(v; I_0, I_1) + h.o.t.. \quad (1.9)$$

Using the expansions for  $I$  and  $w$ , we can now also expand Eqs. 1.1,1.2:

$$f(v, w; I) = f_0(v; I_0) + \epsilon f_1(v; I_0, I_1) + h.o.t., \quad (1.10)$$

$$g(v, w) = g_0(v; I_0) + \epsilon g_1(v; I_0, I_1) + h.o.t. \quad (1.11)$$

Notice that the  $w$  dependence of both  $f$  and  $g$  has been removed, as Eq. 1.9 defines  $w$  as a function of  $v$  and  $I$ . Combining Eqs. 1.1,1.2 yields

$$f(v, w; I) \frac{dw}{dv} = \epsilon g(v, w; I). \quad (1.12)$$

Using the approximations for  $f$  and  $g$  from Eqs. 1.10,1.11, we next examine Eq. 1.12 at order  $O(\epsilon^0)$ :

$$f_0(v; I_0) \frac{dw_0(v; I_0)}{dv} = 0. \quad (1.13)$$

For a non-trivial  $w$ , this means:

$$f_0(v; I_0) \equiv -w_0(v; I_0) - v(v-1)(v-a) + I_0 = 0. \quad (1.14)$$

Eq. 1.14 defines  $w_0(v; I_0)$  to be the  $v$ -nullcline for  $I = I_0$ .

Next, examining Eq. 1.12 at order  $O(\epsilon^1)$  yields

$$f_1(v; I_0, I_1) \frac{dw_0(v; I_0)}{dv} + f_0(v; I_0) \frac{dw_1(v; I_0, I_1)}{dv} = g_0(v; I_0). \quad (1.15)$$

By Eq. 1.14  $f_0(v; I_0) = 0$ , so Eq. 1.15 produces an equation for  $f_1(v; I_0, I_1)$ :

$$f_1(v; I_0, I_1) = \frac{g_0(v; I_0)}{w'_0(v; I_0)} \quad (1.16)$$

where the prime denotes differentiation with respect to  $v$ . Since  $w_0(v; I_0)$  is the cubic  $v$ -nullcline, there are values of  $v$  where  $w'_0(v; I_0) = 0$ . Let  $v_i$  be the local minimum of the  $v$ -nullcline, which for  $a = 0.1$  occurs at

$$v_i = (1 + a - \sqrt{1 - a + a^2})/3 \approx 0.048687. \quad (1.17)$$

For the  $\epsilon$  expansion of  $I$  to remain defined (ie, so that  $f_1$  remains  $O(1)$ ),  $g_0$  must  $\rightarrow 0$  as  $v \rightarrow v_i$ , where

$$g_0(v; I_0) = v - \gamma w_0(v; I_0). \quad (1.18)$$

For  $g_0$  to  $\rightarrow 0$  as  $v \rightarrow v_i$ ,  $w_0$  must  $\rightarrow v_i/\gamma$ . Adding this constraint to Eq. 1.14 determines the value of  $I_0$ :

$$I_0 = \frac{v_i}{\gamma} + v_i(v_i - 1)(v_i - a) \approx 0.051064. \quad (1.19)$$

It is worth noting that  $I_0$  is the value of  $I$  where the  $w$ -nullcline passes through the minimum of the  $v$ -nullcline and a decent zeroth order approximation to the location of the Hopf bifurcation point.

For future use, we will now derive expressions for  $w_1(v; I_0, I_1)$  and  $w'_1(v; I_0, I_1)$  in terms of things we know. First, we can derive a second equation for  $f_1(v; I_0, I_1)$  by expanding the definition of  $f$  in Eq. 1.1 to  $O(\epsilon^1)$ :

$$f_1(v; I_0, I_1) = -w_1(v; I_0, I_1) + I_1 \quad (1.20)$$

Rearranging and substituting for  $f_1$  using Eq. 1.16 yields

$$w_1(v; I_0, I_1) = -\frac{g_0(v; I_0)}{w'_0(v; I_0, )} + I_1. \quad (1.21)$$

Differentiating yields an equation for  $w'_1$ :

$$w'_1(v; I_0, I_1) = -\frac{g'_0(v; I_0)w'_0(v; I_0, ) - g_0(v; I_0)w''_0(v; I_0, )}{[w'_0(v; I_0, )]^2}. \quad (1.22)$$

With these equations in place, we will now continue on to examine Eq. 1.12 at  $O(\epsilon^2)$ :

$$f_2 w'_0 + f_1 w'_1 = g_1. \quad (1.23)$$

Rearranging to isolate  $f_2$  yields

$$f_2 = \frac{g_1 - f_1 w'_1}{w'_0}. \quad (1.24)$$

Again, since  $f$  must remain bounded, as  $w'_0 \rightarrow 0$  so must  $(g_1 - f_1 w'_1)$ . Using Eqs. 1.16, 1.21, 1.22, we can now plug in for  $g_1$ ,  $f_1$ , and  $w'_1$ , yielding a definition for  $I_1$  in terms of known quantities:

$$\begin{aligned} g_1 - f_1 w'_1 &= -\gamma w_1 + \frac{g_0 g'_0 w'_0 - g_0 w''_0}{w'_0 (w'_0)^2} \\ &= -\gamma \left(-\frac{g_0}{w'_0} + I_1\right) + \frac{g_0 g'_0 w'_0 - g_0^2 w''_0}{(w'_0)^3}. \end{aligned} \quad (1.25)$$

Eq. 1.25 must  $\rightarrow 0$  when  $w'_0 \rightarrow 0$ , ie as  $v \rightarrow v_i$ . The only term which is not already defined is  $I_1$ , so we will isolate this term:

$$I_1 = \lim_{v \rightarrow v_i} \left( \frac{g_0 g'_0 w'_0 + \gamma g_0 (w'_0)^2 - g_0^2 w''_0}{\gamma (w'_0)^3} \right), \quad (1.26)$$

where all derivatives are evaluated at  $v = v_i$ . As  $v \rightarrow v_i$ , both the numerator and denominator of Eq. 1.26 go to 0 since both  $g_0$  and  $w'_0$  go to 0. To find the value of  $I_1$  in the limit as  $v \rightarrow v_i$  we apply L'Hospital's rule three times, which using  $g_0 \rightarrow 0$  and  $w'_0 \rightarrow 0$  yields

$$I_1 = \lim_{v \rightarrow v_i} \left( \frac{g'_0(g''_0 w''_0 + 2\gamma(w''_0)^2) - (g'_0)^2 w_0^{(3)}}{2\gamma(w''_0)^3} \right) \approx 0.69405. \quad (1.27)$$

Plugging this value into Eq. 1.8, produces the following approximation for the location of the canard point:

$$I_C \approx I_0 + \epsilon I_1 = 0.05662. \quad (1.28)$$

This result is equivalent to the predicted canard value from (3.23) of Brøns [6].  $I_C$  is accurate to first order in  $\epsilon$ , and matches the numerical result shown in Fig. 1.2 to that order.

# Chapter 2

## Control Method

Our goal is to design a control mechanism that steers the FHN model to the parameter values at which canards occur, without precise foreknowledge of this value. Since  $I$  is the bifurcation parameter in Eqs. 1.1,1.2, it makes a natural control variable as well. Based on Fig. 1.2, if the periodic orbits are large,  $I$  should be decreased and if the periodic orbits are small,  $I$  should be increased. Our control strategy for  $I$  follows this blueprint. If  $I$  is allowed to drift back-and-forth, this strategy would produce MMO, but when properly set up it will pick out the mid-size, canard orbits.

We choose to use continuous feedback control based on the position of the system in phase space, similar to the approach of Moreau and Sontag for tuning to a Hopf bifurcation [43]. The local minimum of the  $v$ -nullcline is the base point for our measurements and we construct a control circle around this point to determine whether trajectories are instantaneously small or large. When a

trajectory is inside the circle, it is considered small and  $I$  should be increased. The opposite is true when a trajectory is outside the circle.  $I$  will cycle over a small range when a trajectory balances the effects of sometimes being inside and sometimes outside the circle.

To include this control strategy in the FHN model, we augment Eqs. 1.1,1.2 with the following differential equation for  $I$ :

$$\dot{I} = c(r_0 - r). \quad (2.1)$$

The new variable  $r = \sqrt{(v - v_i)^2 + (w - w_i)^2}$  is the instantaneous Euclidean distance from the local minimum of the  $v$ -nullcline. The parameters  $c$  and  $r_0$  determine the control strength and radius of the control circle, respectively, and will be tuned to produce a “good” canard. This control strategy is memoryless, as it depends only on the instantaneous position in phase space, and also does not require foreknowledge of the canard point parameter value. That being said, for this control strategy to work the system must begin in an oscillatory region of parameter space, but can start with parameters on either side of the canard point. This control strategy also requires approximate knowledge of the size of periodic orbits on either side of the canard point; setting  $r_0$  to one third of the distance from the local minimum of the  $v$ -nullcline to the local maximum is a reasonable starting point.

It is worth noting that changes in  $I$  cause the intersection of the two nullclines to move, and thus the exact position of  $(v_i, w_i)$  to change. However, as

the changes in  $I$  between the Hopf bifurcation point and the canard region are approximately 0.015 (see Fig. 1.2), the changes to  $v_i$  and  $w_i$ , and thus  $r$  over this range are of the same small order. In the following we have fixed  $v_i = w_i = 0.05$ . As we will discuss in Section 3.1, the control method is robust to far larger changes in the position of the control circle than result from these approximations for  $v_i$  and  $w_i$ .

## 2.1 Comparing the Effectiveness of Strategies

To compare the effectiveness of this control strategy for various values of  $c$  and  $r_0$ , we would like to measure the distance over which the trajectory remains in the neighborhood of the slow manifold  $M_U$ . This manifold is within  $O(\epsilon)$  of the middle portion of the  $v$ -nullcline. This implies that the slope of  $M_U$  must be close to that of  $v$ -nullcline. When a trajectory departs from a neighborhood of  $M_U$ , it does so abruptly making a sharp turn with a large change in slope. With these considerations in mind, our distance measurement begins when the trajectory passes the local minimum of the  $v$ -nullcline. We consider the trajectory to have departed the neighborhood of  $M_U$  when its slope differs by 0.09 from that of the  $v$ -nullcline with the same value of  $v$ . This value, which is an order of magnitude larger than  $\epsilon$ , was chosen so that the trajectory with the longest measurement has a large change in slope just before the local maximum of the  $v$ -nullcline. Fig. 2.1 shows several trajectories and how our method classifies their distance.

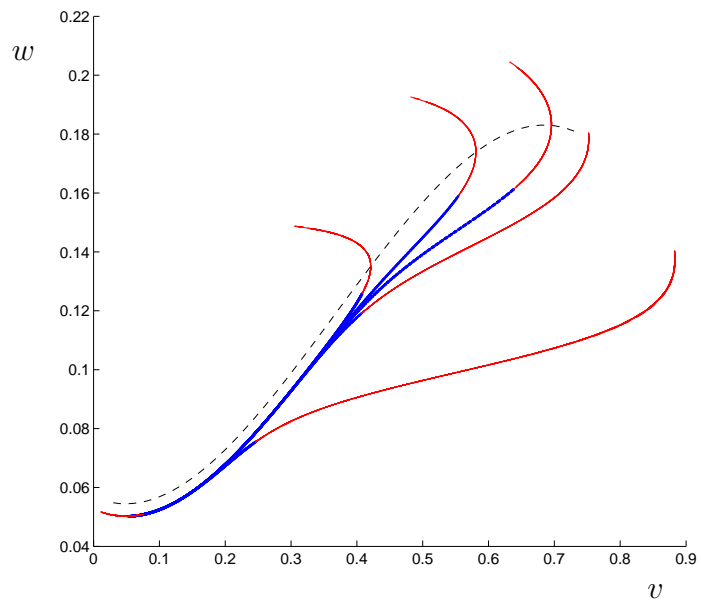


Figure 2.1: Demonstration of how our distance measure classifies several trajectories. The dashed line is the  $v$ -nullcline, within  $O(\epsilon)$  of  $M_U$ . The thicker part of the trajectories count towards the distance following  $M_U$ , the thinner pieces do not. Here, the longest distance is approximately 0.6, the shortest 0.15.

We also tried other methods for measuring the distance near  $M_U$ . Our first attempt was to place an envelope around the  $v$ -nullcline and stop our distance measurement when the trajectory left this envelope. While this strategy was fairly effective, the maximal canard trajectory naturally evolves away from the  $v$ -nullcline at higher values of  $v$ . To properly capture the length of this trajectory requires a fairly generous envelope that counts the initial sections of trajectories that depart from the manifold early. Using a slope based measure allows a gentle progression away from the manifold, while correctly handling sharply divergent trajectories. In principle, it would also be possible to calculate a direct approximation to  $M_U$ . However, the middle section of the  $v$ -nullcline is an  $O(\epsilon)$  approximation of  $M_U$  and proved sufficient for our treatment.

# Chapter 3

## Results

The results of a two parameter study of  $c$  and  $r_0$  using the distance measure from Section 2.1 are shown in Fig. 3.1, where we average over multiple visits near  $M_U$  to account for the possibility of MMO, as described below. Using other values for this slope difference threshold results in a slightly different specific largest canard, but the results are very similar. As  $r_0$  increases from 0.15, then distance over which trajectories remain in the neighborhood of  $M_U$  generally increases until reaching its peak around  $r_0 = 0.234$ . The longest canard orbit in our study occurs for  $c = 1 \times 10^{-8}$  and  $r_0 = 0.234$ , and is shown in Fig. 3.2. Just above this value of  $r_0$ , the length of trajectories drops sharply as the trajectories turn off a shorter distance up  $M_U$ . As the two parameter study shows, using a smaller value of  $c$  produces longer tracking of  $M_U$  and thus more canard-like shapes. Using values of  $c$  below  $1 \times 10^{-8}$  does not significantly improve the distance measure.

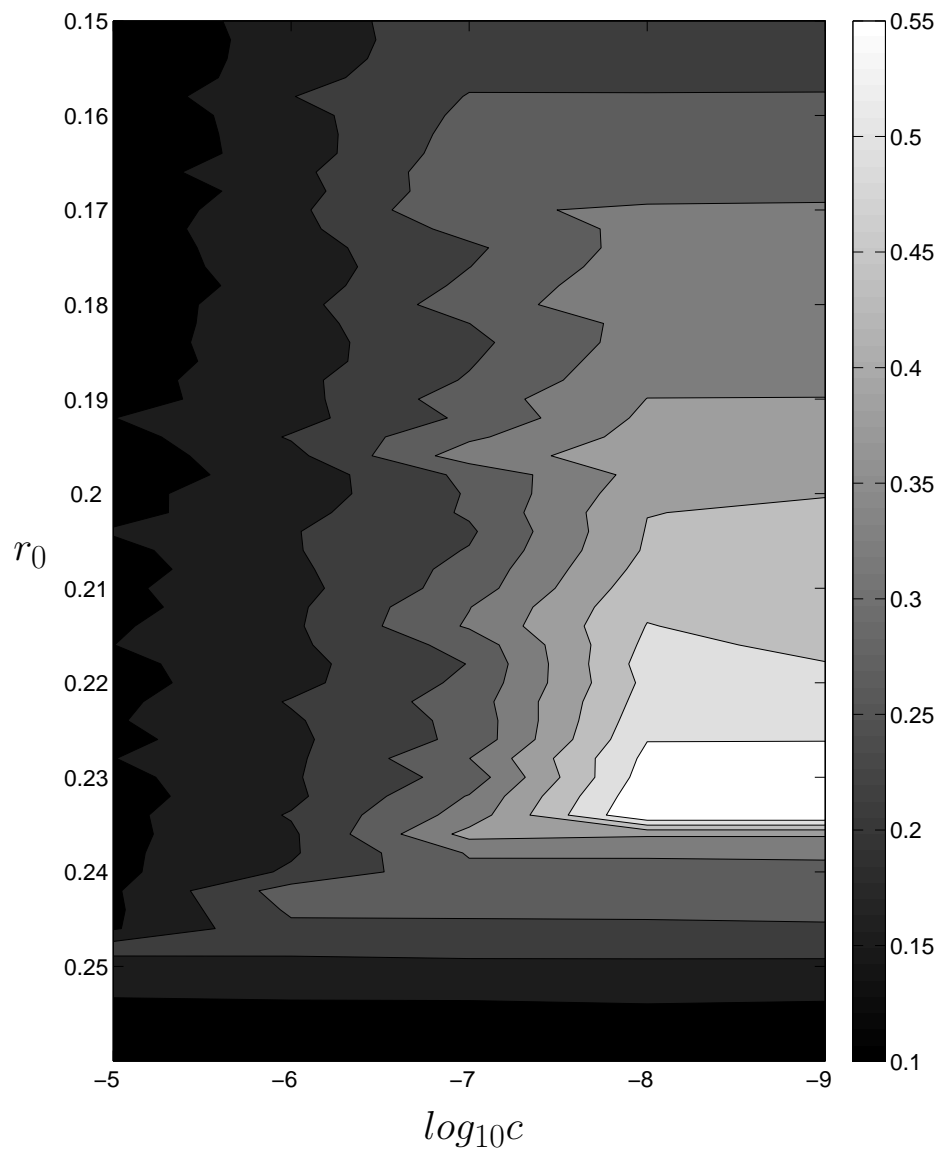


Figure 3.1: Contour plot of the average distance the trajectories remain in the neighborhood of  $M_U$  after transients have died out. Average is taken over at least 40 successive visits near  $M_U$ .

The value of  $c$  must be smaller than  $1 \times 10^{-4}$  to tune the system to the canard region. As demonstrated in Fig. 1.3, the canard region in  $I$  is smaller than  $1 \times 10^{-5}$ , with maximal canards in a range of  $I$  several orders of magnitude smaller. Our choice of memoryless, continuous control also mandates very small corrections. This size constraint on  $c$  effectively creates three time scales for the system 1.1,1.2,2.1, as  $1 \gg \epsilon \gg c$ . Over the maximal canard trajectory, the control parameter  $I$  is never stationary but enters into a repeating cycle as shown in Fig. 3.3. As the trajectory passes near the local minimum of the  $v$ -nullcline, it is in the center of the control circle and  $I$  increases most rapidly. The trajectory then passes out of the circle on its way up  $M_U$ , and  $I$  starts to decrease by larger amounts as the orbit moves through the canard’s “head.” On its return to  $M_S$ , the trajectory briefly passes through the top of the control circle, resulting in the short reversal in Fig. 3.3. As this occurs away from the  $v$ -nullcline, the trajectory is moving quite rapidly, keeping the reversal small.

### 3.0.1 Mixed-Mode Oscillations and Chaos

While the canard trajectory shown in Fig. 3.2 traces a single orbit each time around, this is not always the case. For  $c = 1 \times 10^{-8}$ , we also found MMO with one large and one small orbit, as shown in Fig. 3.4. These MMO occur when the control strategy over-corrects for the value of  $I$ . When the trajectory departs the local minimum of the  $v$ -nullcline headed for a large orbit, it spends

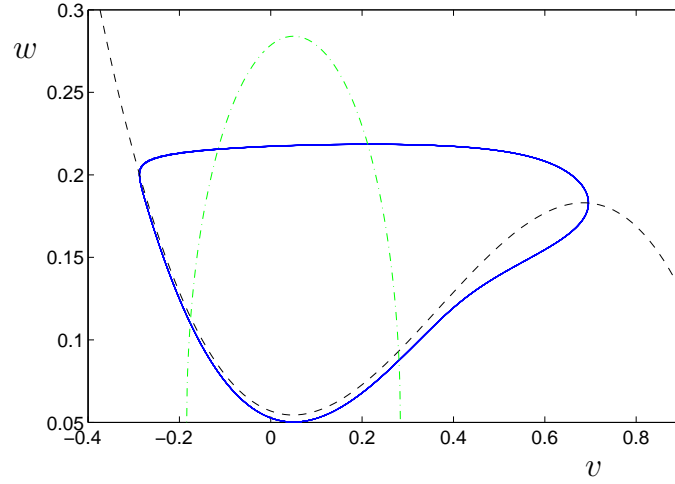


Figure 3.2: This canard trajectory, produced using control with  $c = 1 \times 10^{-8}$  and  $r_0 = 0.234$ , has the longest distance measure along  $M_U$ . The axes are not square, so the dot-dashed control circle appears elliptical.

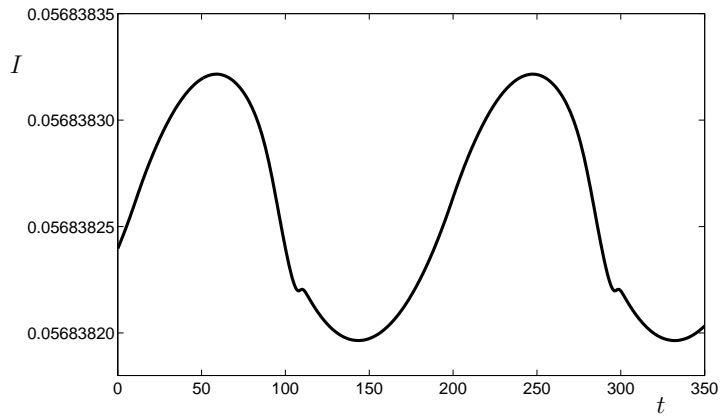


Figure 3.3: Evolution of  $I$  for the trajectory in Fig. 3.2.

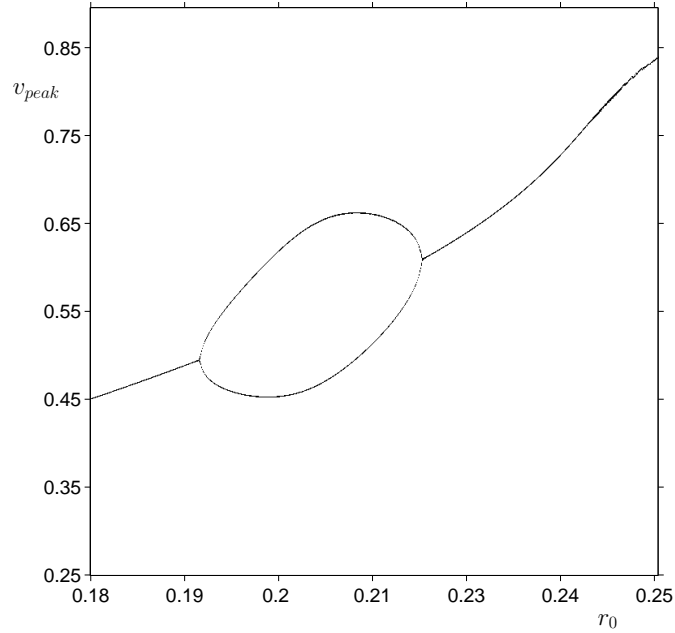


Figure 3.4: Bifurcation diagram for  $c = 1 \times 10^{-8}$  showing peak values of  $v$ , generated by adiabatically increasing the value of  $r_0$ , omitting transients. There is a period two bubble corresponding to a MMO with one small and one large orbit as  $r$  is swept from 0.18 to 0.25. The maximal canard has  $v_{peak} \approx 0.65$ .

a substantial amount of time outside the control circle, which lowers the value of  $I$ . When the trajectory re-enters the control circle,  $I$  begins to increase again. If the control circle is too small and/or the control strength  $c$  too large, then when the trajectory departs again it will have over-corrected the value of  $I$  and lead to a small orbit. The trajectory then spends a substantial amount of time inside the control circle, which increases the value of  $I$  and can lead to another large orbit.

When  $c$  is increased, the window of MMO expands. Figure 3.5 shows bifurcation diagrams for  $c = 2 \times 10^{-8}, 5 \times 10^{-8}, 1 \times 10^{-7}$ . For all three of these, the period doubling “bubble” in Fig. 3.4 expands into cascades of period doubling

bifurcations, that leads to chaotic MMO. As  $c$  increases, the width of the region with complex behavior broadens as the propensity for over-correction in  $I$  increases. The chaotic region is broken up by windows of MMO periodic orbits, with the number of MMO windows increasing with  $c$ . Each of these windows corresponds to a different type of MMO, beginning with  $1^n$  orbits ( $L^s$  means  $s$  small orbits for every  $L$  large orbits) for small values of  $r_0$ , transition through  $1^1$  in the middle of the chaotic region, and end as  $n^1$  orbits, as can be seen best in Fig. 3.5(c). A similar chaotic MMO bifurcation structure has been observed experimentally for the Belousov-Zhabotinski (BZ) reaction in [28], as well as an electrochemical system in [49]. These results are also very reminiscent of results in Petrov et al [46].

Figure 3.6 shows the chaotic trajectory for  $c = 1 \times 10^{-7}$  and  $r_0 = 0.17$  with the associated time series for  $I$ . In Fig. 3.7, the  $(v, w)$ -phase plane is expanded with a third dimension for the control variable  $I$ , creating a three dimensional view of the chaotic trajectory in Fig. 3.6. The  $v$ -nullcline is expanded into the  $I$ -dimension to form a two dimensional folded surface  $S$ , with the line of local minima of the  $v$ -nullcline now referred to as the fold-line  $F$ . This chaotic behavior is not the product of integration error or other noise, as a map from the max value of  $v$  from one orbit to the next is distinctly one dimensional, as shown in Fig. 3.8.

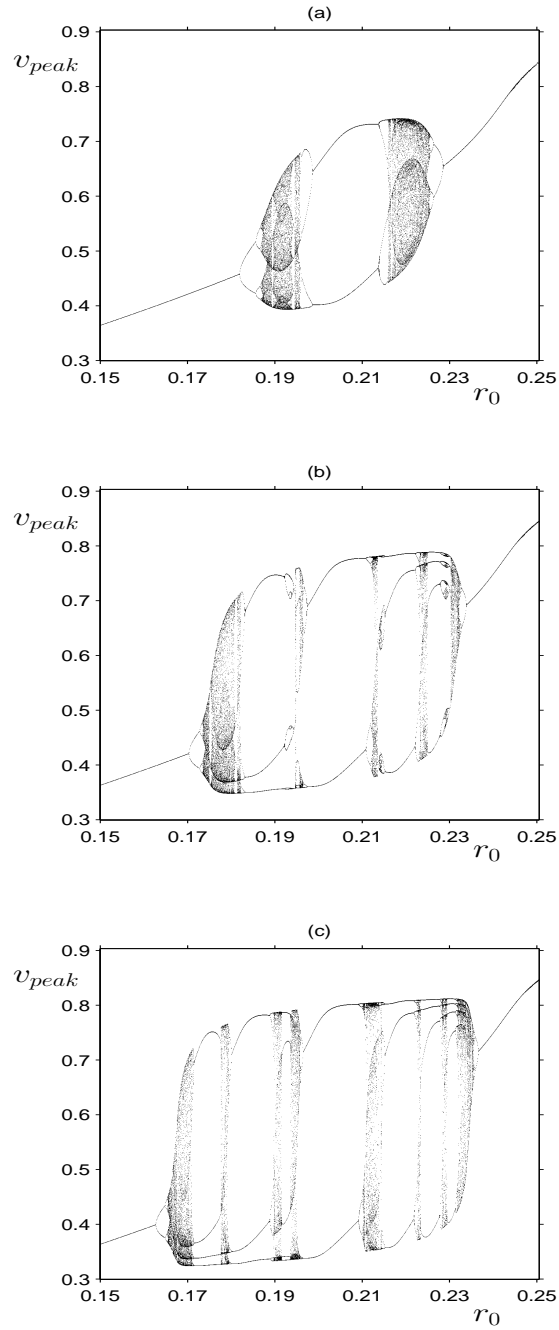


Figure 3.5: Bifurcation diagram, as in Fig. 3.4, for (a)  $c = 2 \times 10^{-8}$ , (b)  $c = 5 \times 10^{-8}$ , (c)  $c = 1 \times 10^{-7}$ , all showing period doubling cascades to chaos and various periodic windows corresponding to periodic MMO. The maximal canard has  $v_{peak} \approx 0.65$ .

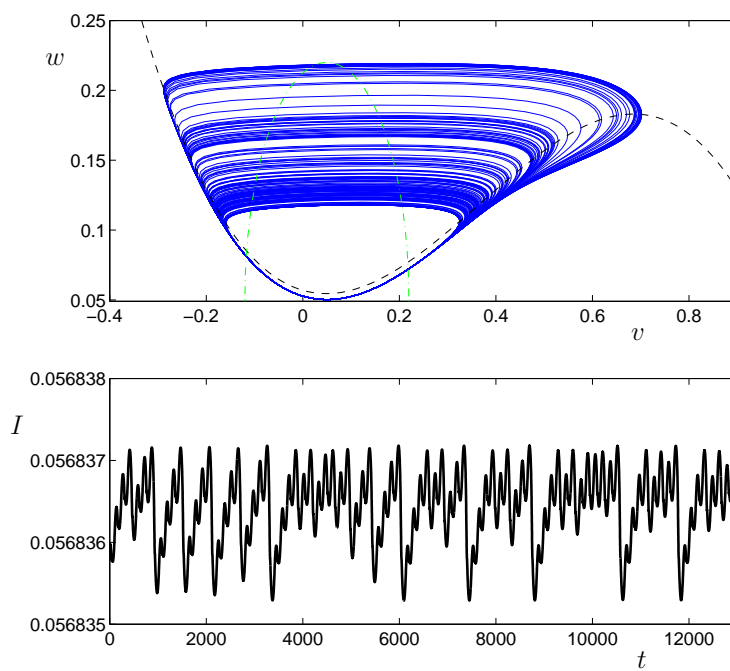


Figure 3.6: Control with  $c = 1 \times 10^{-7}$  and  $r_0 = 0.17$  produces a chaotic MMO.

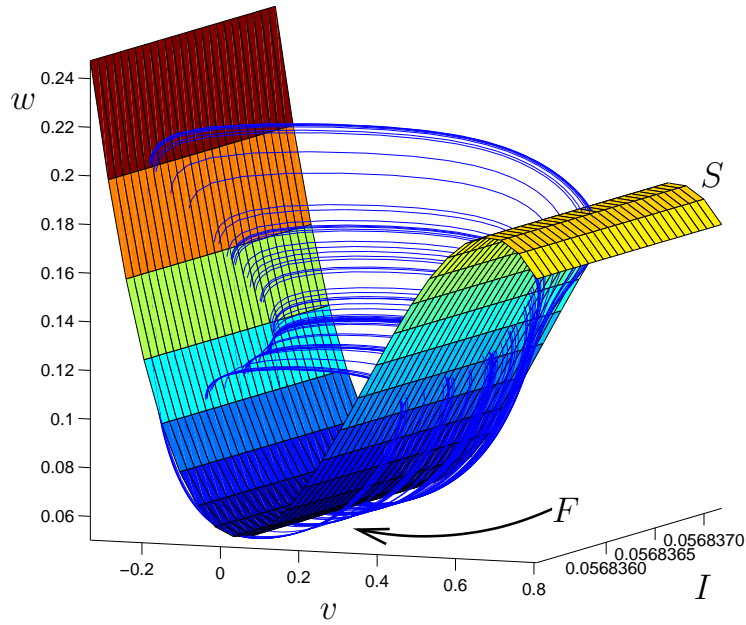


Figure 3.7: Three dimensional representation of the chaotic trajectory from Fig. 3.6, with the  $(v, w)$ -phase plane augmented with a dimension for  $I$ . The cubic  $v$ -nullcline is now the two dimensional surface  $S$  with fold-line  $F$ .

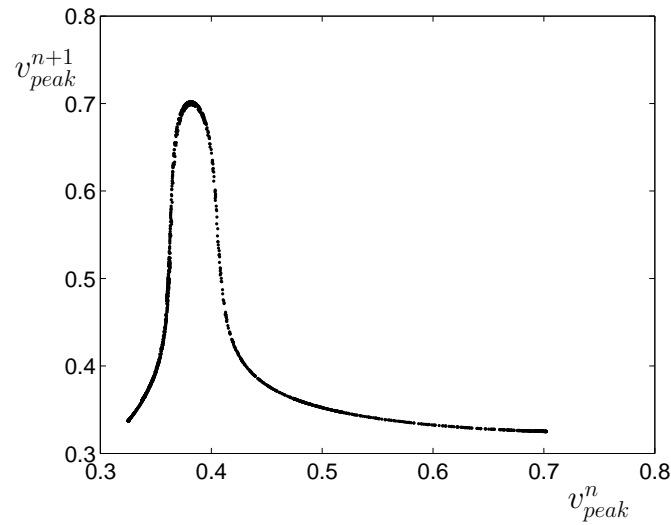


Figure 3.8: Map of peak value of  $v$  in Fig. 3.6 versus the previous peak. This one dimensional map shows that the spread of orbits in Fig. 3.6 is due to chaos.

### 3.1 Robustness

We studied the effects of moving the control circle so it was not centered at  $(0.05, 0.05)$ , the approximate local minimum of the  $v$ -nullcline. The control strategy still functions when the circle is displaced by less than half of  $r_0$ , although the specific best canard or MMO behavior does change when the circle moves. Figure 3.9 shows results for two parameter study like Fig. 3.1 but with the control circle displaced by 0.076 to  $(0.12, 0.08)$ . This plot is almost indistinguishable from that for the centered circle, with only small differences in structure.

These results indicate that the control strategy is robust to small errors or changes in  $v_i$  and  $w_i$ , and effective without precise positioning of the circle. However, if the circle is displaced so it no longer contains the local minimum of the  $v$ -nullcline, the controller cannot work.

Our control method is also robust to large, but infrequent, changes in system properties. For the FHN model, we use steps in  $\gamma$  to simulate these sudden changes. As shown in Fig. 3.10(a), the control method is capable of responding to these changes and locating the new canard region. The time it takes the system to reach the canard window depends on the value of  $c$ , with larger values locating the canard window more quickly while smaller values find it more precisely. To reach the canard region both quickly and precisely, we developed a strategy for adjusting control strength  $c$  depending on past performance of  $I$ .

Essentially, if  $I$  has settled in and continues oscillating over the same re-

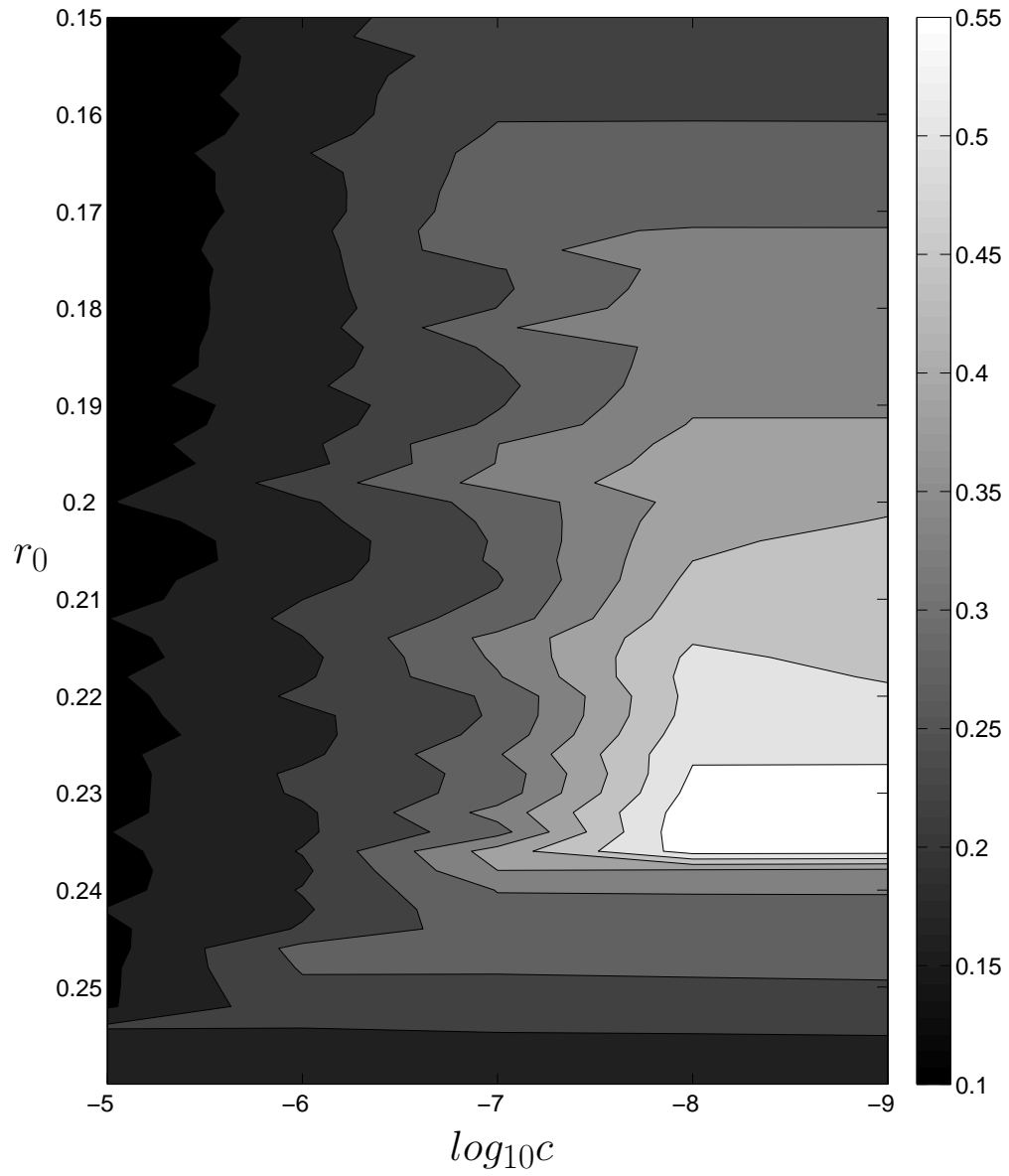


Figure 3.9: Contour plot with the same setup as Fig. 3.1 except that the center of the control circle has been displaced to  $(0.12, 0.08)$ . The two contours are nearly identical despite the translated control circle.

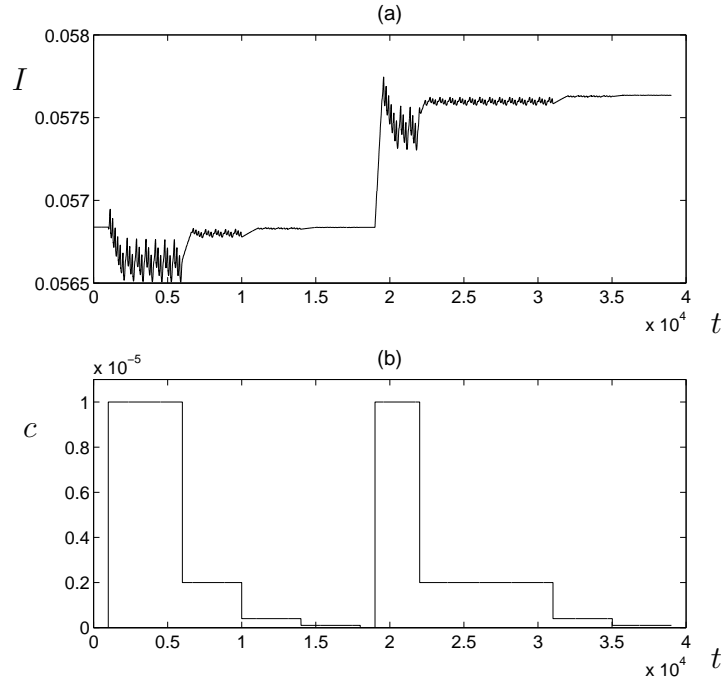


Figure 3.10: (a) Control variable  $I$  first locates initial canard window for  $\gamma = 1.0$ . After it achieves a lock,  $\gamma$  is reduced to 0.985 and  $I$  then tunes to the new canard window at  $I = 0.05764$ , as confirmed by simulations. (b) The control strength  $c$  is varied based on recent history of  $I$ .

gion,  $c$  is reduced to more accurately determine the canard window, as shown in Fig. 3.10(b). If  $I$  is moving in one direction for a sufficiently long time,  $c$  is increased to reduce the time until the new canard window is acquired. This adaptation of  $c$  requires knowledge of past values of  $I$ , but greatly improves the settling time for smaller values of  $c$ . In addition, this adaptation mechanism allows for rapid, precise convergence on the canard region from an initial condition to an unknown value of  $I_C$ .

## 3.2 Simulations With Noise

The high precision required to achieve tuning to a specific canard orbit raises the question of whether the method will work in the presence of noise. One potential source of noise for the FHN neuron model is a noisy external current, which would directly affect the  $v$  equation. Considering Gaussian white noise, Eqs. 1.1,1.2,2.1 are rewritten

$$\dot{v} = -w - v(v-1)(v-a) + I + \sqrt{2D}\eta(t), \quad (3.1)$$

$$\dot{w} = \epsilon(v - \gamma w), \quad (3.2)$$

$$\dot{I} = c(r_0 - r) \quad (3.3)$$

where  $\eta(t)$  represents Gaussian delta-correlated noise with zero mean and unit variance that enters the system continuously.

### 3.2.1 Stochastic Integration method

To simulate the response of our controlled FHN model to white noise, we use a fixed step size, fourth-order Runge-Kutta method adapted for noise from [27]. Consider the general multi-dimensional stochastic system

$$\dot{y} = f(y) + \sqrt{2D}\eta(t), \quad (3.4)$$

where  $y$  is the state vector for the system and  $[\sqrt{2D}\eta(t)]_i = \sqrt{2D_i}\eta_i(t)$  with each  $\eta_i(t)$  representing an independent Gaussian delta-correlated noise with zero

mean and unit variance. Let  $y_0$  be the state the system at time  $t_0$ , and  $f(y_0)$  the associated derivative in the absence of noise. The approximate state at time  $t_0 + h$  is then given by:

$$Y_1 = f(y_0), \quad (3.5)$$

$$Y_2 = f\left(y_0 + \frac{h}{2}Y_1 + \sqrt{hD}\eta(t_2)\right), \quad (3.6)$$

$$Y_3 = f\left(y_0 + \frac{h}{2}Y_2 + \sqrt{hD}\eta(t_3)\right), \quad (3.7)$$

$$Y_4 = f\left(y_0 + hY_3 + \sqrt{hD}\eta(t_4)\right), \quad (3.8)$$

$$y(t_0 + h) \approx y_0 + \frac{h}{6}(Y_1 + 2Y_2 + 2Y_3 + Y_4) + \sqrt{hD}\eta(t_0 + h). \quad (3.9)$$

The different  $t$  values used for  $\eta(t)$  are intended just to indicate that different values of the random noise are used for each expression. See Appendix A for the MATLAB code used for these stochastic simulations.

To select the time step for stochastic simulations of the FHN model, we first simulated Eqns. 1.1,1.2,2.1 without noise using MATLAB's fourth-order Runge-Kutta solver, `ode45`. Setting the error tolerances to  $1 \times 10^{-10}$  allowed the system to settle into the maximal canard orbit. After these noise-less simulations completed, we found the smallest step-size these simulations had required and used a slightly smaller value of 0.1 seconds for the fixed time step in our stochastic simulations.

### 3.2.2 Results With Noise

Under continuous noise, our controller is able to approach  $I$  values close to the canard transition, but is unable to produce canard-shaped orbits. Figure 3.11 shows what happens to the maximal canard in Fig. 3.2 when a small amount of noise is injected. To achieve a canard shape, the trajectory must follow  $M_U$ . Even small amplitudes of white noise cause the trajectory to depart from  $M_U$  and the control logic is simply not set up to offset these local effects. Instead of canard shapes, Eqs. 3.1,3.2,3.3 produce noisy MMO even for tiny noise strengths. This is reminiscent of the noise-induced spiking presented in Makarov, Nekorkin, and Velarde [37]. For our system, larger (resp., smaller) values of noise strength  $D$  move the fork in Fig. 3.11 lower (resp., higher) on  $M_U$ . It is possible to produce similar results to those of Makarov et al using our method. Choose a small value for  $r_0$  (like 0.12) and, in the absence of noise, the control will produce small periodic orbits. With noise, the system will sporadically produce large orbits.

To tune to maximal canard orbits in the presence of noise, perhaps an alternative control method could be developed based on deviation of the orbit from  $M_U$ . This would have the potential to overcome continuous noise, but would require either specific prior information about the canard system or an adaptive memory. The approximation to  $M_U$  would have to be known to high precision and the controller sufficiently powerful to counter the natural deviation from the unstable manifold.

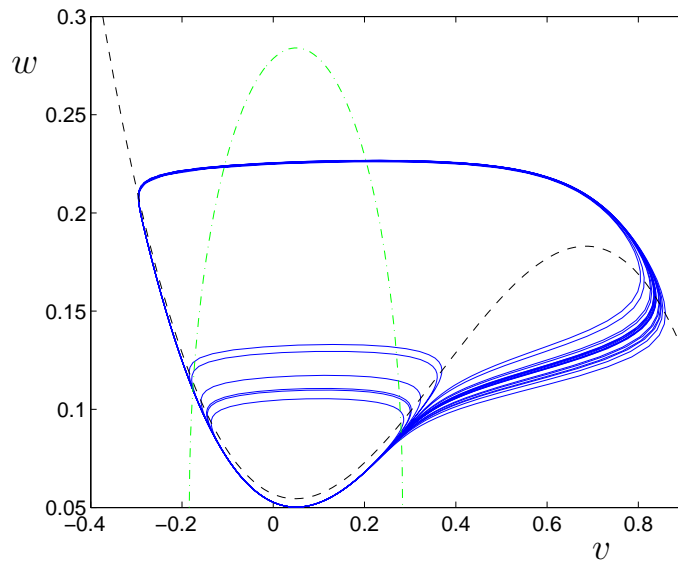


Figure 3.11: Noisy MMO produced using  $c = 1 \times 10^{-8}$ ,  $r_0 = 0.234$  and noise strength  $D = 1 \times 10^{-11}$ . This is the same controller that produced the best canard in Fig. 3.2. With noise, the controller can only find the general location of the canard window; the continuous noise precludes actual canard trajectories.

# Chapter 4

## Conclusion

We have demonstrated a novel technique for inducing the FitzHugh-Nagumo (FHN) model to operate at a canard point. After the addition of a differential equation regulating the parameter  $I$ , the model self-tunes to operate in the canard region. When properly tuned, our continuous, memoryless method produces repeated maximal canard trajectories. Mixed-mode oscillations (MMO), including chaotic trajectories, were observed for suboptimal control setups. While our method can relocate the precise canard region when one of the parameters in the FHN model changes, it can only find the general vicinity of the canard region when subjected to continuous white noise. If noise could be sufficiently minimized, a sensor operating at the canard point could detect minute changes to the operating parameters of the system without the hysteresis issues associated with operating at a subcritical Hopf bifurcation. We note that this control strategy will not stabilize unstable canards, such as a branch of periodic orbits

arising from a subcritical Hopf bifurcation [42].

In future work, several enhancements to the controller could prove beneficial. Adding an integral term to Eq. 2.1 could enable the system to more quickly locate the canard orbit when initialized far from the canard region. Adding damping might achieve a similar result and reduce the prevalence of MMO by shrinking the oscillations in  $I$  for larger values of  $c$ . Several changes would be necessary to counteract continuous white noise, but a controller that estimated the location of  $M_U$  and counteracted deviations away from that manifold might prove successful. It would also be interesting to investigate generalities of this control strategy for higher dimensional systems exhibiting canards, using a control cylinder with axis along the fold line or a hypersphere.

# Bibliography

- [1] S. M. Baer and T. Erneux. Singular Hopf bifurcation to relaxation oscillations. *SIAM J. Appl. Math.*, 46:721–739, 1986.
- [2] S. M. Baer and T. Erneux. Singular Hopf bifurcation to relaxation oscillations II. *SIAM J. Appl. Math.*, 52:1651–1664, 1992.
- [3] E. Benoit, J.-L. Callot, F. Diener, and M. Diener. Chasse au canard. *Collect. Math.*, 32:37–119, 1981.
- [4] K. Bold, C. Edwards, J. Guckenheimer, S. Guharay, K. Hoffman, J. Hubbard, R. Oliva, and W. Weckesser. The forced van der Pol oscillator II: Canard in the reduced flow. *SIAM J. Appl. Dyn. Syst.*, 2:570, 2003.
- [5] M. Brøns. Excitation and annihilation in the FitzHugh-Nagumo equations. *IMACS Trans. Sci. Comp.*, 1.1:297–301, 1989.
- [6] M. Brøns. Relaxation oscillations and canards in a nonlinear model of discontinuous plastic deformation in metals at very low temperatures. *Proc. R. Soc. A*, 461:2289–2302, 2005.

- [7] M. Brøns and K. Bar-Eli. Canard explosion and excitation in a model of the Belousov-Zhabotinsky reaction. *J. Phys. Chem.*, 95:8706–8713, 1991.
- [8] M. Brøns and K. Bar-Eli. Asymptotic analysis of canards in the EOE equations and the role of the inflection line. *Proc. R. Soc. Lond. A*, 445:305–322, 1994.
- [9] M. Brøns, M. Krupa, and M. Wechselberger. Mixed mode oscillations due to the generalized canard phenomenon. *Fields Institute Communications*, 49:39–63, 2006.
- [10] J.-L. Callot, F. Diener, and M. Diener. Le problème de la “chasse au canard”. *C. R. Acad. Sci. Paris (Sér. I)*, 286:1059–1061, 1978.
- [11] S. Camalet, T. Duke, F. Jülicher, and J. Prost. Auditory sensitivity provided by self-tuned critical oscillations of hair cells. *PNAS*, 97(7):3183–3188, 1999.
- [12] J. Cronin. *Mathematical Aspects of Hodgkin-Huxley neural theory*. Cambridge University Press, Cambridge, 1987.
- [13] J. Drover, J. Rubin, J. Su, and B. Ermentrout. Analysis of a canard mechanism by which excitatory synaptic coupling can synchronize neurons at low firing frequencies. *SIAM J. Appl. Math.*, 65(1):69–92, 2004.
- [14] F. Dumortier and R. Roussarie. Canard cycles and center manifolds. *Mem. Amer. Math. Soc.*, 121, 1996.

- [15] W. Eckhaus. Relaxation oscillations including a standard chase on French ducks. *Lecture Notes in Math.*, 985:449–494, 1983.
- [16] V.M Eguíluz, M. Ospeck, Y. Choe, A.J. Hudspeth, and M.O. Magnasco. Essential nonlinearities in hearing. *Phys. Rev. Lett.*, 84(22):5232–5235, 2000.
- [17] V.M Eguíluz, M. Ospeck, Y. Choe, A.J. Hudspeth, and M.O. Magnasco. Evidence of a Hopf bifucation in frog hair cells. *Biophysical Journal*, 80(6):2597–2607, 2001.
- [18] I. R. Epstein and K. Showalter. Nonlinear chemical dynamics: oscillations, patterns, and chaos. *J. Phys. Chem.*, 100:13132, 1996.
- [19] N. Fenichel. Persistence and smoothness of invariant manifolds for flows. *Indiana Univ. Math. Journal*, 21:193–226, 1971.
- [20] N. Fenichel. Geometric singular perturbation theory for ordinary differential. *J. Diff. Eq.*, 31:53–98, 1979.
- [21] R. FitzHugh. Mathematical models of threshold phenomena in the nerve membrane. *Bull. Math. Biophysics*, 17:257–278, 1955.
- [22] R. FitzHugh. Impulses and physiological states in theoretical models of nerve membrane. *Biophysical J.*, 1:445–466, 1961.
- [23] R. Fitzhugh. *Mathematical models of excitation and propagation in nerve*, chapter 1, pages 1–85. McGraw-Hill Book Co, N.Y., 1969.

- [24] V. Gáspár and K. Showalter. A simple model for the oscillatory iodate oxidation of sulfite and ferrocyanide. *J. Phys. Chem.*, 94:4973–4979, 1990.
- [25] J. Guckenheimer, K. Hoffman, and W. Weckesser. Numerical computation of canards. *Int. J. Bif. Chaos*, 10:2669–2687, 2000.
- [26] A. L. Hodgkin and A. F. Huxley. A quantitative description of membrane current and its application to conduction and excitation in nerve. *J. Physiol.*, 117:500–544, 1952.
- [27] R. L. Honeycutt. Stochastic Runge-Kutta algorithms. *Phys. Rev. A*, 45(2):604–610, 1992.
- [28] J. L. Hudson, M. Hart, and D. Marinko. An experimental study of multiple peak periodic and nonperiodic oscillations in the BelousovZhabotinskii reaction. *J. Chem. Phys.*, 71:1601, 1979.
- [29] E. M. Izhikevich. *Dynamical Systems in Neuroscience: The Geometry of Excitability and Bursting*. The MIT Press, Cambridge, MA, 2007.
- [30] E. M. Izhikevich and R. FitzHugh.  
[http://www.scholarpedia.org/article/fitzhugh-nagumo\\_model](http://www.scholarpedia.org/article/fitzhugh-nagumo_model).
- [31] J. Keener and J. Sneyd. *Mathematical Physiology*. Springer, New York, 1998.

- [32] M. T. M. Koper. Bifurcations of mixed-mode oscillations in a three-variable autonomous Van der Pol-Duffing model with a cross-shaped phase diagram. *Physica D*, 80(1):72–94, 1995.
- [33] M. Krupa and P. Szmolyan. Extending geometric singular perturbation theory to nonhyperbolic points - fold and canard points in two dimensions. *SIAM J. Math. Anal.*, 33:286–314, 2001.
- [34] M. Krupa and P. Szmolyan. Relaxation oscillation and canard explosion. *J. Diff. Eq.*, 174:312–368, 2001.
- [35] E. Sontag L. Moreau and M. Arcak. Feedback tuning of bifurcations. *System and Control Letters*, 50:229–239, 2003.
- [36] M. O. Magnasco. A wave traveling over a Hopf instability shapes the cochlear tuning curve. *Phys. Rev. Lett.*, 90(5):058101, 2003.
- [37] V. A. Makarov, V. I. Nekorkin, and M. G. Velarde. Spiking behavior in a noise-driven system combining oscillatory and excitatory properties. *Phys. Rev. Lett.*, 86:3431, 2001.
- [38] F. Marino, G. Catalán, P. Sánchez, S. Balle, and O. Piro. Thermo-optical ‘canard orbits’ and excitable limit cycles. *Phys. Rev. Lett.*, 92:073901, 2004.
- [39] G. S. Medvedev and J. E. Cisternas. Multimodel regimes in a compartmental model of the dopamine neuron. *Physica D*, 194:333–356, 2004.

- [40] A. Milik, P. Szmolyan, H. Löffelmann, and E. Gröller. Geometry of mixed-mode oscillations in the 3-D autocatalator. *Int. J. Bif. Chaos*, 8:505–519, 1998.
- [41] J. Moehlis. Canards in a surface oxidation reaction. *J. Nonlin. Sci.*, 12:319–345, 2002.
- [42] J. Moehlis. Canards for a reduction of the Hodgkin-Huxley equations. *J. Math. Biol.*, 52:141, 2006.
- [43] L. Moreau and E. Sontag. Balancing at the border of instability. *Phys. Rev. E*, 68:020901, 2003.
- [44] J. Nagumo, S. Arimoto, and S. Yoshizawa. An active pulse transmission line simulating nerve axon. *Proc IRE*, 50:20612070, 1962.
- [45] B. Peng, V. Gáspár, and K. Showalter. False bifurcations in chemical systems: canards. *Phil. Trans. R. Soc. Lond. A*, 337:275–289, 1991.
- [46] V. Petrov, S. K. Scott, and K. Showalter. Mixed-mode oscillations in chemical systems. *J. Chem. Phys.*, 97(10):6191–6198, 1992.
- [47] J. Rinzel. Excitation dynamics: insights from simplified membrane models. *Federation Proc.*, 44:2944–2946, 1985.
- [48] H. G. Rotstein, N. Kopell, A. M. Zhabotinsky, and I. R. Epstein. Canard

- phenomenon and localization of oscillations in the Belousov-Zhabotinsky reaction with global feedback. *J. Chem. Phys.*, 119:8824, 2003.
- [49] M. Schnell and F. N. Albahadily. Mixed-mode oscillations in an electrochemical system. *J. Chem. Phys.*, 90(2):822–828, 1989.
- [50] S. Schuster and M. Marhl. Bifurcation analysis of calcium oscillations: Time-scale separation, canards, and frequency lowering. *J. Biol. Syst.*, 9:291, 2001.
- [51] P. Szmolyan and M. Wechselberger. Canards in  $R^3$ . *J. Diff. Eq.*, 177:419–453, 2001.
- [52] M. Wechselberger. Existence and bifurcation of canards in  $R^3$  in the case of a folded node. *SIAM J. Appl. Dyn. Syst.*, 4:101, 2005.
- [53] S. Wiggins. *Normally Hyperbolic Invariant Manifolds in Dynamical Systems*. Springer, New York, 1994.

# Appendix A

## Appendix

The following MATLAB function performs stochastic integration using a fourth order Runge-Kutta method.

```
function [PlotTime,PlotVars] = RK4wN(InitialConds,tSpan,
    h,saveInc,noiseStrength,funcHandle)
% Input variables:
% InitialConds: Vector of initial states for all
%   variables in question
% tSpan: [startTime, endTime]
% h: Size of fixed time steps
% saveInc: Save a point for plotting every saveInc steps
% noiseStrength: magnitude of noise to subject simulation to
% funcHandle: Handle for a vector function that,
%   given inputs [State], returns vector of first
%   derivatives for each state
% Output variables:
% PlotTime: Vector of timesteps (to ease plotting)
% PlotVars: Matrix with states values at each timestep,
%   final value is final state

    Time = tSpan(1);
    State = InitialConds;

    % Filling out defined length arrays is far faster
    % than dynamic resizing
```

```

numSavePts = ceil(tSpan(2)/(h*saveInc) + 1);
PlotTime = zeros(numSavePts,1);
PlotVars = zeros(numSavePts,length(InitialConds));
PlotTime(1,1) = tSpan(1);
PlotVars(1,:) = InitialConds;

numPoints = 0;
saveIndex = 1;

% Loop through time steps
while( Time < tSpan(2) - 1E-8 )
    % Find next state, increment time
    [State,Time] = TimeStepper(State,Time,h,noiseStrength,
        funcHandle);
    % Save values for plotting
    if( mod( numPoints, saveInc ) == 0 )
        saveIndex = saveIndex + 1;
        PlotTime(saveIndex) = Time;
        PlotVars(saveIndex,:) = State;
    end

    numPoints = numPoints + 1;
end

FinalState = State;

function [Final,FinalTime] = TimeStepper(Initial,Time,h,
    noiseStrength,funcHandle)
    % Find next state using user supplied function
    Y1 = funcHandle(Initial);
    Y2 = funcHandle(Initial + h/2*Y1 +
        sqrt(noiseStrength*h)*randn(1));
    Y3 = funcHandle(Initial + h/2*Y2 +
        sqrt(noiseStrength*h)*randn(1));
    Y4 = funcHandle(Initial + h*Y3 +
        sqrt(noiseStrength*h)*randn(1));

    Final = Initial + h/6*(Y1+2*Y2+2*Y3+Y4) +
        sqrt(noiseStrength*h)*randn(1);
    FinalTime = Time + h;

```